Accelerated Bayesian optimization in deep cooling atoms

Xiaoxiao Ma(马笑笑), Changwen Liang(梁昌文), Rong Sha(沙荣), Chao Zhou(周超), Guochao Wang(王国超), Jixun Liu(刘纪勋), Shuhua Yan(颜树华), Lingxiao Zhu(朱凌晓)

Citation: Chin. Phys. B. 35, 100205 (2026). DOI: 10.1088/1674-1056/ae24ef | CSTR: 32038.14.CPB.ae24ef
http://cpb.iphy.ac.cn; http://iopscience.iop.org/cpb

What follows is a list of articles you may be interested in

Sequential noise-boosted M-estimation for robust parameter estimation under impulsive noise

Li Zhang(张莉), Yan Pan(潘燕), Fabing Duan(段法兵), François Chapeau-Blondeau, Derek Abbott
Chin. Phys. B. 35, 030204 (2026). DOI: 10.1088/1674-1056/adfefe | CSTR: 32038.14.CPB.adfefe

A Yb optical clock with a lattice power enhancement cavity

Chunyun Wang(王春云), Yuan Yao(姚远), Haosen Shi(师浩森), Hongfu Yu(于洪浮), Longsheng Ma(马龙生), Yanyi Jiang(蒋燕义)
Chin. Phys. B. 33, 030601 (2024). DOI: 10.1088/1674-1056/ad1986

Mutation detection and fast identification of switching system based on data-driven method

Zhonghua Zhang(张钟化), Wei Xu(徐伟), Yi Song(宋怡)
Chin. Phys. B. 32, 050201 (2023). DOI: 10.1088/1674-1056/acb9f5

Accelerated Bayesian optimization in deep cooling atoms

Xiaoxiao Ma(马笑笑)[†], Changwen Liang(梁昌文)[†], Rong Sha(沙荣)[†], Chao Zhou(周超), Guochao Wang(王国超), Jixun Liu(刘纪勋), Shuhua Yan(颜树华), and Lingxiao Zhu(朱凌晓)[‡]

College of Intelligence Science and Technology, National University of Defense Technology, Changsha 410073, *China*

(Received 25 October 2025; revised manuscript received 23 November 2025; accepted manuscript online 27 November 2025)

Laser cooling, which cools atomic and molecular gases to near absolute zero, is the crucial initial step for nearly all atomic gas experiments. However, fast achievement of numerous sub-μK cold atoms is challenging. To resolve the issue, we propose and experimentally validate an intelligent polarization gradient cooling approach enhanced by an optical lattice, utilizing maximum hypersphere compensation sampling Bayesian optimization (MHCS-BO). MHCS-BO demonstrates a twofold increase in optimization efficiency and superior prediction accuracy compared to conventional Bayesian optimization. Finally, approximately 10^8 cold atoms at a temperature of 0.4±0.2 μK can be achieved given the optimal parameters within 15 minutes. Our work provides an intelligent protocol, which can be generalized to other high-dimensional parameter optimization problems, and paves the way for the preparation of ultracold atoms in quantum experiments.

Keywords: deep cooling atoms, laser cooling, Bayesian optimization, optical lattice

PACS: 02.60.Pn, 03.75.Be

DOI: 10.1088/1674-1056/ae24ef **CSTR:** 32038.14.CPB.ae24ef

1. Introduction

Atomic cooling plays a crucial role in various quantum systems,[1] including quantum precision measurement,[2,3] quantum simulation,[4] and quantum information.[5] Atomic cooling methods include magneto-optical trap (MOT) cooling,[6] polarization gradient cooling (PGC),[7] evaporative cooling,[8] Raman sideband cooling,[9] and so on. Among these, PGC stands out as a cheap approach that could obtain lower atomic temperature simply by designing the timing sequence without the need for extra hardware. Research indicates that in quantum metrology based on cold atomic interferometry, lower atomic temperature could improve interference fringe contrast and measurement sensitivity.[10] While conventional PGC is fundamentally limited to the μK regime, evaporative cooling can prepare Bose–Einstein condensation (BEC) at the nK level. However, the generation of BEC usually requires demanding hardware (*e.g.*, high-power optical trap) and exhibits low efficiency,[11] which is a critical limitation incompatible with the demand for high measurement frequency in quantum metrology. Thus, the efficient preparation of sub-μK cold atoms holds critical importance for enhancing atomic interferometer performance and enabling engineering applications. With the aid of an optical lattice for adiabatic cooling, the atomic temperature could be further reduced.[12] However, the process of preparing cold atoms is quite complex, highly nonlinear, and susceptible to environmental influences. Conventional manual optimization results in low accuracy and efficiency, making it difficult to control the cooling process more finely due to the complexities associated with high-dimensional optimization. It is also particularly challenging to ensure a lower temperature while maintaining a higher atomic number.

Recently, artificial intelligence (AI) has been applied to solve optimization problems involving quantum systems.[13] Evolutionary algorithms such as genetic algorithm,[14] differential evolution,[15] and particle swarm optimization,[16] can search for globally optimal parameters. However, these algorithms, usually depending on large population scales and iteration steps, work inefficiently in scenarios with high experimental cost. Neural networks (NNs) such as multilayer perceptron,[17] deep learning,[18] and reinforcement learning[19] are applicable to high-dimensional multi-objective optimization problems. Similar to evolutionary algorithms, NNs also require a large amount of experimental data to train networks. The accuracy of NNs extremely requires a robust system and high-quality datasets. Fortunately, Bayesian optimization (BO)[20–22] can efficiently optimize parameters, especially in complex systems with high experimental cost. The acquisition function, e.g., expected improvement (EI), probability of improvement, and upper confidence bound, could obtain good optimization effects in the majority of scenarios. Nevertheless, traditional acquisition functions always leave large non-sampling regions in parameter space, compromising the predictive performance of the model in high dimension.

In our previous work,[23] we utilized reinforcement learning (RL) to optimize the PGC sequence, demonstrating superior cooling performance over manual tuning while validating the feasibility of intelligent fine control over the PGC process.

[†]These authors contributed equally to this work.

[‡]Corresponding author. E-mail: zhulingxiao31@163.com

© 2026 Chinese Physical Society and IOP Publishing Ltd. All rights, including for text and data mining, AI training, and similar technologies, are reserved.

In this study, we implement one-dimensional (1D) deep cooling along the vertical direction assisted by an optical lattice to obtain sub-μK cold atoms. The increased system complexity and strong parameter coupling increase the cost of the objective function, which would lead to lower efficiency using the RL framework. We utilize Bayesian optimization (BO) to address this challenge. As an efficient global optimization framework well-suited for expensive objective functions, BO demonstrates superior optimization efficiency compared to evolutionary algorithms and neural networks.[24] Furthermore, we make improvements to the traditional BO and propose maximum hypersphere compensation sampling Bayesian optimization (MHCS-BO) to perform stepwise decoupled optimization of the cooling process. It is illustrated that MHCS-BO has twice the optimization efficiency and higher prediction accuracy than traditional BO. As a result, lower atomic temperature and more sufficient atoms can be obtained. In the experiment, the cooling process is divided into 10 segments to be finely controlled, and thus a total of 16 experimental parameters are optimized in a decoupled manner by MHCS-BO. Approximately 10^8 cold atoms at a temperature of 0.4 ± 0.2 μK can be obtained with 15 minutes of MHCS-BO.

2. Results and discussion

The experimental setup is mainly composed of a three-dimensional (3D)-MOT, laser systems, a vacuum chamber, and a controller (Fig. 1(c)). The laser system can be found in Note 1 of the supplementary information. The cooling beam has a radius of about 26 mm, a power of about 14 mW, and is red-detuned by 15 MHz from the $|F=2\rangle \rightarrow |F'=3\rangle$ transition. A Gaussian beam with a power of about 30 mW, red detuning of approximately 67 GHz from $|F=2\rangle \rightarrow |F'=3\rangle$ transition, and diameter of around 1.8 mm (forming potential well with depth about $15T_r$–$30T_r$, where $T_r \approx 0.362$ μK is the recoil temperature), is incident into the vacuum chamber, reflected by a mirror to form a 1D optical lattice at the center of the MOT. A charge-coupled device (CCD) camera is mainly used to observe the atomic cloud during operation and measure the atomic temperature. The light used for detection of time-of-flight (TOF) signal is shaped by a 100 mm×1 mm aperture. When atomic cloud passes through this region, the resonant fluorescence could be detected by a photonic detector (PD) and conveyed to the host computer by a 16-bit data acquisition card.

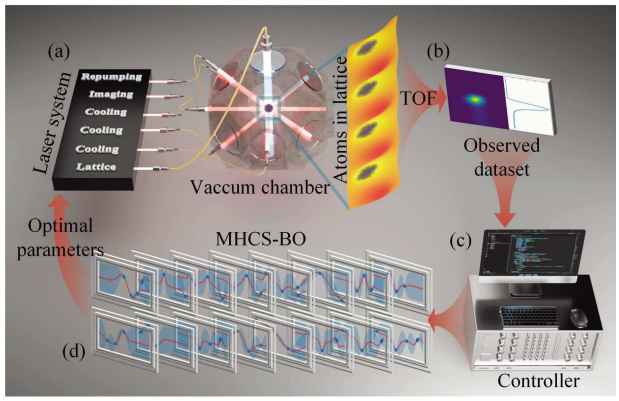

Fig. 1. Experiment diagram: (a) the atoms are trapped in a 3D MOT, where the PGC assisted by optical lattice can be achieved through controlling the experimental parameters such as magnetic field, laser power, and detuning. The 1D optical lattice is formed by two red detuning laser beams, with intensity distribution following Gaussian and harmonic profile along the radial and axial directions respectively. (b) When the atomic cloud falls across detection zone, TOF signal is generated, which can be utilized to calculate the objective function. A host computer executes the MHCS-BO algorithm with observed dataset (d), predicting the optimal parameters which are utilized in the laser system through the controller (c).

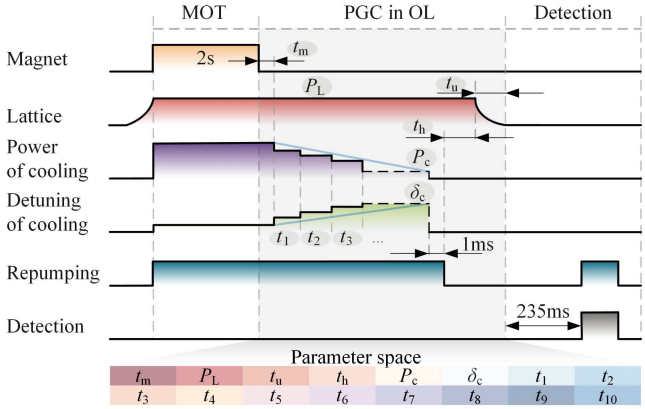

Fig. 2. Timing sequence and parameters space. OL: optical lattice; t_m: time to turn off magnetic coils; P_L: power of lattice light; t_u: duration of the optical lattice unloading; t_h: holding time of optical lattice; P_c: power of cooling light at the end of PGC; δ_c: detuning of cooling light at the end of PGC; t_i $(i=1,2,\ldots,10)$, the time step of PGC. The MOT loads for a duration of 2 seconds, followed by the starting of PGC after a delay of t_m. The atoms are then pumped to the $|F=2\rangle$ state by turning off the repumping light 1-ms later than the cooling light. After being released from lattice, the atoms undergo a 235-ms free-falling in vacuum chamber before reaching the detection zone, which is about 270 mm blew the center of MOT.

Setting reasonable parameters $\boldsymbol{X}$, one experiment cycle can be conducted following the timing sequence depicted in Fig. 2. Consequently, the TOF signal can be obtained on the host computer. The atomic temperature T_a is acquired by fitting the TOF signal in the velocity domain (see Note 5 of the supplementary information for details), which is subsequently used to calculate the objective function $O(\boldsymbol{X})$. A pairwise observed data point consisting of scaled parameters $\boldsymbol{X}$ and corresponding $O(\boldsymbol{X})$ would be used to fit the surrogate model, which is a Gaussian process in this study. MHCS-BO is utilized to predict the optimal parameters for the next experiment cycle. The above process iterates until reaching the termination criterion. To finely control the process of PGC, we discarded the linear changing of cooling light parameters in traditional PGC (blue line). Instead, the PGC interaction time is divided into 10 steps, and each step t_i $(i=1,2,\ldots,10)$ is a variable to be optimized. The initial power and detuning of the cooling light in PGC are the same as those in the MOT stage, and are subsequently changed to P_c and δ_c at the termination of the PGC stage. There is a time delay t_m between MOT and PGC. By adjusting t_i, P_c, and δ_c, the power and detuning can have different sequences, achieving fine control of the PGC

process. After the completion of PGC, only the lattice light continues to hold on for a certain time t_h and then unloads adiabatically within time t_u to achieve a lower T_a. However, if t_h is too long, atoms will be accelerated due to gravity and the lattice, leading to a decrease in the atomic number N_a within the potential well. Additionally, the power of the lattice light P_L can affect the well depth and scattering rate. A deep well results in more confined atoms, but the velocity distribution of atoms will be widened, resulting in a higher T_a. Conversely, a shallow well corresponds to fewer N_a and a lower T_a. Moreover, a higher scattering rate, which means a higher probability of interaction between atoms and photons, would elevate the probability of atom heating. Thus, t_h and P_L are key parameters that need to be optimized and balanced.

In summary, the parameters that need optimization are $\boldsymbol{X} = \{P_c, \delta_c, t_i, t_m, t_u, t_h, P_L\}$ (16 dimensions). As P_c is controlled by an acousto-optic modulator (AOM), its value can be directly controlled by setting the attenuation (Att) of the radio-frequency signal. P_L is controlled by another AOM with its radio-frequency signal provided by an arbitrary waveform generator, and the signal amplitude is modulated by the voltage V_L provided by the controller. We use Att and V_L to replace P_c and P_L (see Note 8 of the supplementary information for details). Therefore, the actual parameters for optimization are $\boldsymbol{X}_a = \{Att, \delta_c, t_i, t_m, t_u, t_h, V_L\}$. If all parameters are optimized together in a coupled manner, it could easily lead to poor signals, misleading the optimization direction. Hence, we first turn off the optical lattice and optimize the PGC-related parameters $\boldsymbol{X}_P = \{Att, \delta_c, t_i, t_m\}$ to initially cool the atoms to below 5 μK. Subsequently, we turn on the lattice and optimize the lattice-related parameters $\boldsymbol{X}_L = \{t_h, t_m, t_u, V_L\}$ to achieve deep cooling of the atoms. It is noteworthy that the magnetic field delay parameter t_m also has some impact on the cooling effect in the optical lattice; thus, it is included in $\boldsymbol{X}_L$. The attenuation coefficient, light power, time, and voltage are measured in dB, mW, ms, and V, respectively.

MHCS-BO is proposed to find the optimal parameters as shown in Fig. 3. The Gaussian process is fitted initially by the dataset, which could be obtained from prior data or randomly sampled in parameter space. The prediction stage is mainly composed of two steps: (i) prediction based on the EI function, (ii) prediction based on MHCS. The corresponding optimal points $\boldsymbol{X}_{EI}$ and $\boldsymbol{X}_{MHCS}$ would be implemented in the apparatus, yielding the objective functions O_{EI} and O_{MHCS} respectively, all of which would be added to the observed dataset. Compared to traditional EI, MHCS can improve the distribution of sampling points and enhance the ability to explore parameter space. To balance T_a and N_a, the objective function is defined as $O(\boldsymbol{X}) = T_a/A_s^b$, where $A_s \propto N_a$ represents the amplitude of the TOF signal, and b is a balancing coefficient within the range of 0.1–1. A higher b prioritizes maximizing atomic numbers, whereas a lower b emphasizes minimizing atomic temperature. To ensure sufficient atomic numbers while pursuing deep cooling, we empirically set $b = 0.5$, which strikes a balanced compromise between these competing goals. To evaluate the impact of random factors such as atomic number fluctuations, atomic temperature variations, and detection noise on $O(\boldsymbol{X})$, 800 experiments are conducted independently, and the system exhibits good long-term stability (see Note 6 of the supplementary information for details). Considering both optimization efficiency and the probabilistic modeling capability of Gaussian processes, we performed only a single measurement per data point during the optimization iterations. As the iteration process runs, the fitted Gaussian process would be more accurate in reflecting the mapping relationship between the experimental parameters and the corresponding $O(\boldsymbol{X})$. Additionally, to assess the performance and generalizability of MHCS-BO, we apply it to 5 standard test functions[25] (see Note 4 of the supplementary information for details). Here, the optimization accuracy is characterized by the historical optimum values recorded during iterative episodes. The results reveal that MHCS-BO outperforms traditional BO, with nearly double the optimization speed and superior prediction accuracy as shown in Fig. 4.

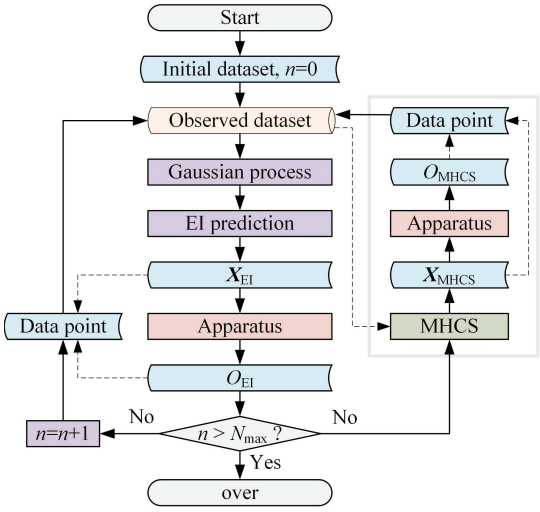

Fig. 3. Flowchart of MHCS-BO. The light blue blocks represent the data generated during optimization process, the red blocks indicate implementing parameters to apparatus and conducting one experiment, the purple blocks depict critical steps in BO, and the gray frame indicates MHCS prediction.

Here, as for the 16 parameters in our experiment, we first provide an intuitive comparison of the optimization efficiency among three methods: MHCS-BO, manual optimization (MO), and brute-force search. MHCS-BO requires decoupling and optimizing the parameters step by step, running a total of 200 experiments, taking about 15 minutes. The MO similarly comprised two steps. For PGC, only the cooling laser power and detuning at the termination stage of PGC were adjusted following the light-blue sequence in Fig. 2. Cooling performance is assessed via fluorescence images of the

atomic cloud after 10 ms–25 ms of free fall, where smaller and brighter images corresponded to higher atomic numbers and lower temperatures. Based on the optimized PGC configuration, the optical lattice parameters are then optimized by observing the TOF signal similar to that in Fig. 5(d). The process was inherently dependent on prior experience and less efficient than algorithmic approaches. Even when MO is operated by an experienced operator familiar with the system, it typically takes 4–6 hours to obtain satisfactory results. In the context of grid brute-force search, employing a parameter step size of $P_{\text{range}}/3$ (P_{range} is the parameter range), which denotes a coarse granularity, necessitates conducting an impractical number of 3^{16} experiments, equivalent to an estimated duration of approximately 6 years. As a result, MHCS-BO is appropriate for our experiment.

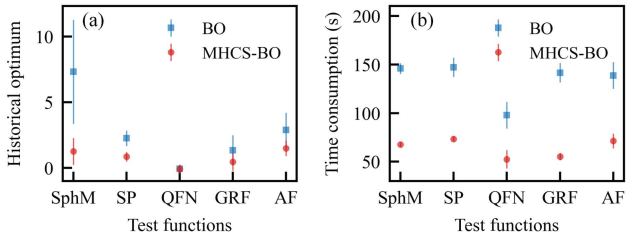

Fig. 4. Performance comparison between MHCS-BO and BO under 5 typical test functions. The historical optimum (a) and time consumption (b) under different test functions are displayed. Each data is averaged by 9 repetitions, and the error bars indicate one standard deviation. SphM: sphere model, SP: Schwefel's problem 2.21, QFN: quartic function *i.e.*, noise; GRF: generalized Rastrigin's function, AF: Ackley's function.

The optimization results under different conditions are illustrated in Fig. 5. The impact of BO and MHCS-BO on the optimization process of PGC is compared in Fig. 5(a). The iterations for BO and MHCS-BO are set to 100 and 50, respectively, yielding 100 sampling points. It can be observed that in the vast majority of iterations, the EI prediction line in MHCS-BO is significantly lower than that in BO, indicating that MHCS-BO can obtain promising parameters. This implies that exploration of non-sampling sparse regions by the MHCS effectively enhances the completeness of the observed dataset, bringing a more precise mapping from the model to the apparatus, resulting in greatly improved EI prediction performance. MHCS-BO and BO reach the historical global optimum at the 61st and 66th samples, respectively.

The historical global optimal parameters for MHCS-BO are $\boldsymbol{X}_{\text{P}}^{*} = \{31.5, 188.21, 10.0, 6.42, 2.37, 5.25, 0.9, 0.42, 9.96, 7.76, 1.04, 0.3, 6.87\}$. Setting the PGC parameters $\boldsymbol{X}_{\text{P}} = \boldsymbol{X}_{\text{P}}^{*}$, $\boldsymbol{X}_{\text{L}}$ is optimized while keeping the lattice light holding on. The results are depicted in Fig. 5(b). The majority of the best values are generated by EI predictions, which is similar to Fig. 5(a). This suggests that MHCS predictions serve as effective supplements to EI predictions, which play a role in exploring the blind areas in the parameter space, thereby enhancing the overall performance of the model. However, there is still one MHCS prediction point appearing in the historical best value (gray solid line), indicating that the MHCS algorithm has a certain probability of exploring potential optimal values that the EI algorithm cannot predict, highlighting the necessity of the MHCS algorithm. The entire iterative process reaches the historical global optimum at the 63rd sample with $\boldsymbol{X}_{\text{L}}^{*} = \{4.75, 9.76, 0.6, 4.16\}$. It is noteworthy that the magnetic field delay t_{m} here is different from that in $\boldsymbol{X}_{\text{P}}^{*}$, changing from 6.87 ms to 4.75 ms. The last optimal parameters are $\boldsymbol{X}^{*} = \boldsymbol{X}_{\text{P}}^{*}(1:12) \cup \boldsymbol{X}_{\text{L}}^{*}$.

The optimal T_{a} and N_{a} of PGC obtained by MHCS-BO and MO are 3.1 μK, 4.3 μK, and 4.2×10^{8}, 3.6×10^{8} as shown in Fig. 5(c), respectively. Although MO can also achieve a relatively acceptable temperature and atomic number, the optimization process relies on the intuition and familiarity of the system. In other words, different individuals may obtain different optimization results, leading to a degree of subjectivity. In contrast, MHCS-BO executes optimization more objectively and accurately based on $O(\boldsymbol{X})$, resulting in significantly higher optimization metrics compared to MO. With the optical lattice holding on and the parameters set to $\boldsymbol{X}^{*}$, the TOF signals are compared between MHCS-BO and MO. Due to the finite potential depth of the optical lattice, some hotter atoms escape and begin falling first under gravity. In contrast, the colder atoms remain trapped, as the potential is sufficient to counteract gravity, and only start falling after the optical lattice is turned off. Therefore, a dual-peak structure is observed in Fig. 5(d), corresponding to the two distinct atom clouds arriving at the detection zone at different times, respectively. Consequently, the peak of the TOF signal exhibits a relative lag. Moreover, the TOF signal for atoms confined within the optical lattice displays a significantly narrower width, indicating a better cooling effect. The optimal T_{a} and N_{a} inside the optical lattice for MHCS-BO and MO are 0.91 μK, 0.82 μK, and 1.6×10^{8} and 7.1×10^{7}, respectively. With the assistance of the optical lattice, MO also achieves an acceptable atomic temperature, but the atomic number is lower than that of MHCS-BO. This is because we have set a comprehensive optimization metric that balances both T_{a} and N_{a}, rather than solely optimizing the atomic temperature.

In order to verify the necessity of parameter decoupling, we compare the optimization under parameter coupling (OPC) and decoupling (OPD) as shown in Fig. 5(e). Overall, $O(\boldsymbol{X})$ of OPC is generally worse than that of OPD. In our experiments, T_{a} cannot be calculated if the TOF signal is poor. In such an instance, it is directly assigned the value of 100. As a result, the mapping accuracy between the model and the apparatus may be compromised, potentially misleading the optimization direction and slowing down the optimization efficiency. It can be seen that some poor TOF signals are gener-

ated in some samples under OPC. Conversely, such a signal cannot be found in OPD. The optimal T_a and N_a inside the optical lattice from OPC are 1.18 μK and 1.2×10^7, respectively, as depicted in Fig. 5(f), even worse than the ones from MO. Additionally, $O(\boldsymbol{X})$ in OPC fluctuates more significantly than in OPD, indicating it is more susceptible to the environment. Therefore, the overall performance of OPD surpasses that of OPC.

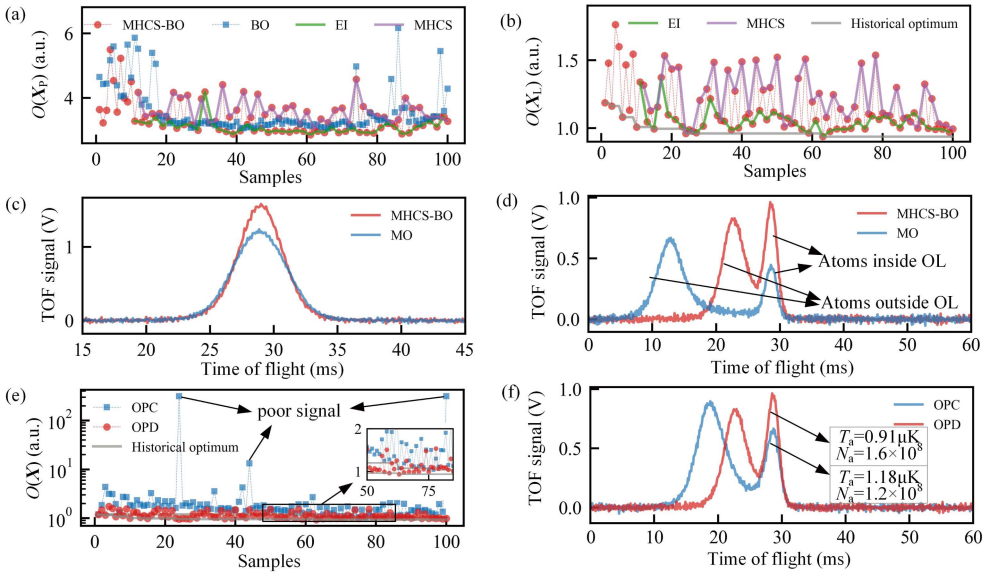

Fig. 5. Optimization of PGC and optical lattice. (a) The optimization of PGC using two different BO algorithms. (b) The MHCS-BO algorithm is used to optimize the 4 parameters of optical lattice. Panels (c) and (d) show the TOF signals of cold atomic clouds under the optimal parameters when optical lattice is closed and open, with the red lines indicating the MHCS-BO results and the blue lines representing the MO results. (e) The BO process under OPC and OPD conditions, where the gray lines represent their respective historical optimum. (f) The best optimization results under OPC and OPD conditions. In panels (c), (d), and (f), the time zero corresponds to the trigger moment of acquisition card, at which point the atomic cloud has been falling for approximately 205 ms after the optical lattice is switched off.

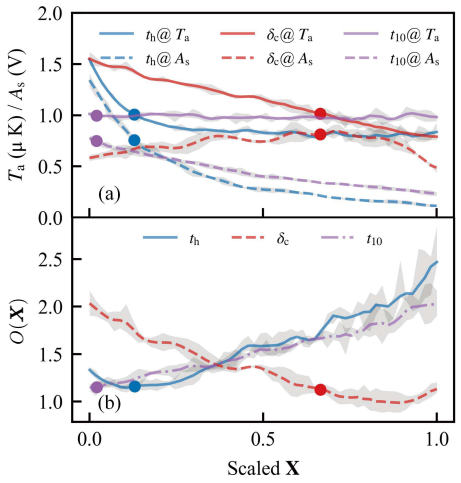

Fig. 6. Key parameter scans under optimal settings. When one parameter changes, the remaining ones are kept at $\boldsymbol{X}^*$, indicated by solid dots in corresponding colors. Each data represents the average of 3 measurements, and the gray area donates one standard deviation. (a) The changing of T_a (solid line) and A_s (dashed line) *versus* scaled parameters. (b) Variation of $O(\boldsymbol{X})$ versus scaled $\boldsymbol{X}$.

Considering the existence of systematic error and random error, the actual experimental parameters may deviate from the setting value. Therefore, it is crucial to ensure that our experimental results, generated by optimal parameters with a few deviations, are proximal to the optimum. Each parameter is scanned under the optimum ($\boldsymbol{X}^*$). Here, only the three parameters that have the greatest impact on cooling effects are analyzed as shown in Fig. 6. The results for other parameters can be seen in Note 7 of supplementary information for details. As the holding time t_h increases, both T_a and A_s decrease (blue line). This phenomenon aligns with physical intuition, because the dipole force, scattering force, and gravity all act on the atoms within the optical lattice. As a result, some atoms escape from the potential well, leading to a decrease in the number of atoms inside the trap. The remaining atoms are those with kinetic energy less than the well depth, which means a lower atomic temperature. With the further extension of t_h, T_a will gradually stabilize. When δ_c gradually increases (red line), there is no apparent pattern in the changes of T_a and A_s. Overall, when δ_c is not too large, T_a decreases with increasing δ_c, while A_s exhibits the opposite trend.

The t_{10} represents the final time step of PGC. As this value increases, A_s decreases gradually, while the change in T_a is less pronounced (purple line). This phenomenon indicates that the atoms have already been sufficiently cooled in the preceding time steps. Therefore, extending the value of t_{10} is equivalent to increasing t_h, resulting in a corresponding alignment between the trends in T_a and A_s with the analysis of t_h. Since $O(\boldsymbol{X})$ is based on T_a and A_s, the lowest atomic temperature was not set as the optimization target. Instead, a balance between them was considered. The position of the optimal parameter can vividly reflect this, indicating that

the objective function has achieved the intended purpose. As shown in Fig. 6(b), the changes of $O(\boldsymbol{X})$ in the vicinity of the optimal point are relatively smooth, without abrupt gradient shifts. This implies that the optimal parameters $\boldsymbol{X}^*$ predicted by MHCS-BO do not coincidentally fall on a singular optimal point and demonstrate a certain degree of robustness, highlighting the superiority of the algorithm proposed in this paper for optimizing multiple parameters in PGC.

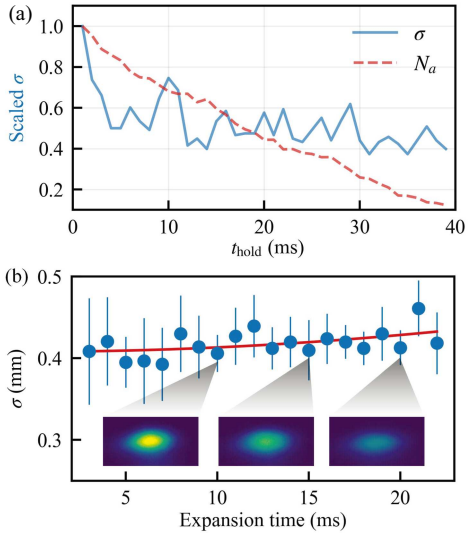

Fig. 7. (a) Scaled σ and N_a *versus* t_h. σ is the Gaussian radii of the atomic cloud, which is obtained by fitting the fluorescence image along vertical direction. A smaller σ means a corresponding lower atomic temperature. N_a is calculated by integrating the counts of fluorescence image. (b) Mean radii of atomic cloud versus expansion time. Each data is averaged by 10 repetitions, and the error bars indicate the standard deviation. The insets is fluorescence images of atomic cloud taken during ballistic expansion. The loading time is adjusted to 3 seconds in order to enhance the detection signal, while the exposure time of CCD camera is set at 0.5 ms.

In order to further explore lower T_a, we increase t_h under the optimal parameters obtained from MHCS-BO. However, as t_h increased, the number of atoms gradually decreased. This would lead to some problems in the measurement of atomic temperature. On one hand, the weakened atomic fluorescence degrades TOF signal fitting precision. On the other hand, the reduced atomic cloud size compromises temperature measurement accuracy, because the thickness of the probe light could not be omitted (see Note 5 of the supplementary information for details). Therefore, we increase the MOT loading time to 3 seconds to obtain more atoms, and employ the ballistic expansion method to precisely measure atomic temperature. By setting t_h to 20 ms, a lower T_a could be achieved without a significant decrease in N_a as depicted in Fig. 7(a). Under this condition, images of the atomic cloud at different expansion times t were captured by a CCD camera. The relationship between the radius of the atomic cloud σ and the expansion time t could be expressed as $\sigma^2 = \sigma_0^2 + (k_B T_a/m)t^2$.[26] Here, σ_0 is the initial radius of the atomic cloud, k_B is the Boltzmann constant, and m is the mass of the ^{87}Rb atom. By fitting the above equation as shown in Fig. 7(b), T_a can be obtained as 0.4±0.2 μK, very close to the recoil temperature.

3. Conclusion

In summary, we have provided the first demonstration of MHCS-BO used in preparing sub-μK cold atoms through PGC assisted with an optical lattice. MHCS-BO inherits the merits of BO, enhances the prediction accuracy, and accelerates the optimization of experimental parameters. Compared to BO, MO, and grid brute-force search, MHCS-BO exhibits significant superiority in rapidly predicting optimal experimental parameters. Within 15 minutes of optimization, the temperature of atoms in the 780-nm optical lattice is 0.4±0.2 μK with an atomic number of 10^8. For the first time, hundreds of millions of cold atoms close to the recoil temperature are created, and it can be extended to 3D cooling by adding another lattice beam. One limitation of MHCS-BO, however, is that it cannot find the complete Pareto frontier in multi-objective optimization problems. Thus, future iterations could use multi-objective BO to overcome this limitation. Overall, this study demonstrates a new scheme to generate high-quality sub-μK cold atoms, providing insights for initial cooling of cold atom experiments, *e.g.*, BEC, quantum computing, and quantum simulation.

Acknowledgements

Project supported by the National Natural Science Foundation of China (Grant Nos. 12404556 and 62103426) and the Major Sci-Tech Program of Hunan Province, China (Grant No. 2023ZJ1010).

References

[1] Lu Y, Zhang R, Song C, Chen C, Si R and Ning C 2023 *Chin. Phys. Lett.* **40** 093101
[2] Peters A, Chung K Y and Chu S 1999 *Nature* **400** 849
[3] Cimini V, Valeri M, Polino E, Piacentini S, Ceccarelli F, Corrielli G, Spagnolo N, Osellame R and Sciarrino F 2023 *Adv. Photon.* **5** 016005
[4] Ciavarella A N, Caspar S, Singh H and Savage M J 2023 *Phys. Rev. A* **107** 042404
[5] Cao A, Eckner W J, Lukin Yelin T, Young A W, Jandura S, Yan L, Kim K, Pupillo G, Ye J, Darkwah Oppong N and Kaufman A M 2024 *Nature* **634** 315
[6] Kasevich M and Chu S 1991 *Phys. Rev. Lett.* **67** 181
[7] Eytemaee S and Haljan P C 2017 *Phys. Rev. Lett.* **119** 043001
[8] Wang Y, Li Y, Wu J, Liu W, Hu J, Ma J, Xiao L and Jia S 2021 *Opt. Express* **29** 13960
[9] Zohar E, Florshaim Y, Zilberman O, Stern A and Sagi Y 2022 *Phys. Rev. A* **106** 063111
[10] Debs J E, Altin P A, Barter T H, Döring D, Dennis G R, McDonald G, Anderson R P, Close J D and Robins N P 2011 *Phys. Rev. A* **84** 033610
[11] Xu W, Sumarac T, Qiu E H, Peters M L, Cantú S H, Li Z, Menssen A, Lukin M D, Colombo S and Vuletić V 2024 *Phys. Rev. Lett.* **132** 233401
[12] Wei C and Kuhn C C N 2018 *J. Mod. Opt.* **65** 1226

[13] Wigley P B, Everitt P J, van den Hengel A, Bastian J W, Sooriyabandara M A, McDonald G D, Hardman K S, Quinlivan C D, Manju P, Kuhn C C N, Petersen I R, Luiten A N, Hope J J, Robins N P and Hush M R 2016 *Sci. Rep.* **6** 25890

[14] Rohringer W, Bücker R, Manz S, Betz T, Koller Ch, Göbel M, Perrin A, Schmiedmayer J and Schumm T 2008 *Appl. Phys. Lett.* **93** 264101

[15] Palittapongarnpim P, Wittek P, Zahedinejad E, Vedaie S and Sanders B C 2017 *Neurocomputing* **268** 116

[16] Che H, Li A, Fang J, Chen X and Qin F J 2022 *AIP Advances* **12** 075211

[17] Liu Q, Xie Y, Li L, Liang A, Li W, Chen H, Fang S, Qu Q, Liu L, Wang B and Lü D 2021 *Chin. J. Lasers* **48** 2412001

[18] Tranter A D, Slatyer H J, Hush M R, Leung A C, Everett J L, Paul K V, Vernaz-Gris P, Lam P K, Buchler B C and Campbell G T 2018 *Nat. Commun.* **9** 4360

[19] Reinschmidt M, Fortágh J, Günther A and Volchkov V V 2024 *Nat. Commun.* **15** 8532

[20] Barker A J, Style H, Luksch K, Sunami S, Garrick D, Hill F, Foot C J and Bentine E 2020 *Mach. Learn.: Sci. Technol.* **1** 015007

[21] Wei J, Wu D, Dong T, Zu C, Xia Y and Yin J 2025 *Chin. Phys. B* **34** 063701

[22] Yang Z, Wang X, Xu H, Li X, Zhu S and Chen H 2025 *Chin. Phys. Lett.* **42** 014302

[23] Liang C, Gao S, Liu J, Wang G, Yan S, Yang J, Zhu L and Ma X 2024 *Opt. Express* **32** 40364

[24] Anton O, Henderson V A, Da R E, Sekulic I, Burger S, Schneider P I and Krutzik M 2024 *Mach. Learn.: Sci. Technol.* **5** 025022

[25] Yao X, Liu Y and Lin G 1999 *IEEE Trans. Evolut. Comput.* **3** 82

[26] Wang X and Sun Y 2023 *Chin. J. Sci. Instrum.* **44** 70